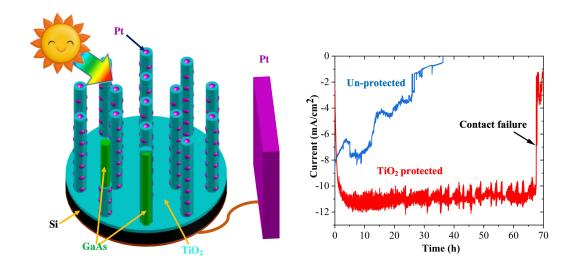
Robust Protection of III-V Nanowires in Water Splitting by a Thin Compact TiO2 Layer

Fan Cui^{1†}, Yunyan Zhang^{1,8†*}, H. Aruni Fonseka², Premrudee Promdet³, Ali Imran Channa⁴, Mingqing Wang⁵, Xueming Xia³, Sanjayan Sathasivam³, Hezhuang Liu⁴, Ivan P. Parkin³, Hui Yang⁶, Ting Li⁷, Kwang-Leong Choy^{5*}, Jiang Wu^{4*}, Chris Blackman³, Ana M. Sanchez² & Huiyun Liu¹

- Department of Electronic and Electrical Engineering, University College London, London WC1E 7JE, UK
- 2. Department of Physics, University of Warwick, Coventry CV4 7AL, United Kingdom
- 3. Department of Chemistry, University College London, London WC1H 0AJ, UK
- Institute of Fundamental and Frontier Sciences, University of Electronic Science and Technology of China, Chengdu 610054, P. R. China
- UCL Institute for Materials Discovery, University College London, Roberts Building, Malet Place, London, WC1E 7JE, UK.
- Department of Materials, Imperial College London, Exhibition Road, London SW7 2AZ,
 UK
- Institute of Biomedical Engineering, Chinese Academy of Medical Sciences & Peking Union
 Medical College, Tianjin, 300192
- Department of Physics, Paderborn University, Warburger Straße 100, 33098, Paderborn,
 Germany
- † These authors contributed equally to this work.
- *E-mail: yunyan.zhang.11@ucl.ac.uk, k.choy@ucl.ac.uk, jiangwu@uestc.edu.cn



Abstract: Narrow-bandgap III-V semiconductor nanowires (NWs) with a suitable band structure and strong light-trapping ability are ideal for high-efficiency low-cost solar watersplitting systems. However, due to their nanoscale dimension, they suffer more severe corrosion by the electrolyte solution than the thin-film counterparts. Thus, short-term durability is the major obstacle for using these NWs for practical water splitting applications. Here, we demonstrated for the first time that a thin layer (~7 nm thick) of compact TiO₂ deposited by atomic layer deposition can provide robust protection to III-V NWs. The protected GaAs NWs maintain 91.4% of its photoluminescence intensity after 14 months of storage in ambient atmosphere, which suggests the TiO₂ layer is pinhole-free. Working as a photocathode for water splitting, they exhibited a 45% larger photocurrent density compared with un-protected counterparts and a high Faraday efficiency of 91%, and can also maintain a record-long highlystable performance among narrow-bandgap III-V NW photoelectrodes; after 67 hours photoelectrochemical stability test reaction in strong acid electrolyte solution (pH = 1), they show no apparent indication of corrosion, which is in stark contrast to the un-protected NWs that are fully failed after 35-hours. These findings provide an effective way to enhance both stability and performance of III-V NW based photoelectrodes, which are highly important for practical applications in solar-energy-based water splitting systems.

Key words: III-V nanowires, water splitting, thin TiO2 protection, long-term stability

Introduction

Solar energy is abundant, clean, and renewable, which makes it one of the most promising renewable energy sources that can solve the worldwide energy crisis and the serious environmental problems caused by the combustion of fossil fuels ¹. Solar-driven water-splitting can harvest solar energy and directly convert it into chemical energy, such as hydrogen from water reduction ². Dihydrogen has high energy density, which is beneficial for energy storage and transportation, and is particularly attractive as an energy carrier ³⁻⁵. The combustion of hydrogen to water does not cause any environmental pollution. Hydrogen generation by photoelectrochemical (PEC) water splitting has thus gained great attention ^{4,6-9}.

PEC water splitting requires a thermodynamic potential of ~1.23 eV and ~0.95 eV for full and Z-scheme half water splitting, respectively ^{10–12}. A potential much larger than these values will lead to low energy conversion efficiency due to energy loss ¹⁰. For example, the ZnO with a large band gap of 3.37 eV can only covert a very small portion of high-energy photons in the solar spectrum. Thus, the high-efficiency semiconductor photo-electrode needs to have a narrow bandgap as close as possible to these ranges to convert a larger portion of energy from the solar spectrum ^{13–16}. The bandgap in many III-V semiconducting materials lie in this region.

Their direct bandgap allows high-efficiency photon absorption, making them suitable for high efficiency solar water splitting (~20%) ¹⁷. However, III-V materials are relatively rare and expensive for extensive use. Innovations are needed to harvest solar energy with greater economic viability. The ideal solution is to build the high-efficiency III-V cells onto the low-cost mature Si platform. However, after 20 years of research, the lattice and thermal expansion coefficient mismatches between III-V epi-layers and Si substrates are still hindering the effective implementation of this idea ¹⁸.

III-V nanowire (NW) structures have demonstrated many novel mechanical, optical and electronic properties that are not present in the thin-film counterparts ^{19,20}. High-quality NWs can be grown on inexpensive substrates such as Si, graphene, carbon nanotubes, fibre-textured silicon thin film, amorphous Si, glass, and indium tin oxide, to significantly reduce the overall device cost ²¹. They can also behave as optical antennas ²² to concentrate light as they can greatly enhance the light absorption cross-section (up to 12 times) compared to their physical size ²³. NW arrays can also increase light-scattering due to their subwavelength dimensions ²⁴, resulting in the internal light path lengths up to 73 times longer compared with that of their thin-film counterparts ²⁵. Therefore, NW arrays have advanced light trapping ability, allowing to use a small amount of expensive III-V material and achieve as efficient optical absorption as thick bulk counterparts ²⁶. Moreover, the large surface-to-volume ratio of NWs provide lower the barrier for chemical reaction ⁴. Thus, III-V NW based photoelectrodes for water splitting have attracted great attention. ^{27,28}

Severe photo-induced corrosion of III-V materials in the electrolyte solution is a common problem, and III-V NWs with a nano-scale size are even more vulnerable ²⁹⁻³¹. Due to the unique 1-dimensional structure, they are much more difficult to protect. The lifetime of the unprotected NW water splitting cells is commonly less than 1 day that is far too short to have practical applications ³¹. Titanium dioxide (TiO₂) is one of the most common protection layer materials that is stable over a wide range of pH and potentials ^{18,32}. It also forms a type-II heterojunction with most III-V materials and serves as an effective hole blocking layer while allowing the transport of electrons to the surface for water splitting ^{10,33}. This allows it to reduce the carrier loss by non-radiative surface recombination, and effectively improve the quantum efficiency ³². Thus, it has been widely used in III-V thin-film devices, and has demonstrated quite robust protection against electrolyte corrosion ³⁴. When grown by atomic layer deposition (ALD), it can conformably cover 3-dimensional sample surface with a uniform and precise thickness, therefore giving good protection to III-V NW during the water splitting process. Despite some initial studies ³³, there is still a lack of reports on the achievement of a long-term stability when directly using TiO₂ protection for III-V NWs for water splitting. The thick TiO₂ layers of tens of nanometres or even hundreds of nanometres that have been used to achieve long lifetime protection, lead to parasitic light absorption and poor charge transfer characteristics ^{34,35}. Moreover, the increase in TiO2 thickness can also increase the overpotential with a linear rate of ~21 mV/nm, which results in an additional voltage loss ^{36,37}. Therefore, it is important to develop a robust protection technique using a thin (sub 10 nm) layers of TiO₂ ^{38,39}.

In this study, the protective behaviour of a very thin TiO₂ layer on III-V NWs was studied in depth. With TiO₂ protection, the GaAs NW photocathode demonstrated greatly improved

performance and a record long durability in the photoelectrochemical reaction among narrow-bandgap III-V NWs. This solves a major challenge for using narrow-bandgap III-V NWs in the water splitting for environmentally clean and renewable energy generation.

Results and discussion

Structural Information

GaAs NWs were grown by molecular beam epitaxy (MBE) via self-catalysed mode on p-type Si substrates 40 . The majority of NWs are standing vertically on the substrate as can be seen in the scanning electron microscope (SEM) image in Figure 1a. They are $\sim 10~\mu m$ in length with a diameter of $\sim 300~nm$ at the bottom, which gradually increase to $\sim 550~nm$ at tip. The lower two thirds of the NW is zinc blende crystal structure with occasional single twins, as can be seen in the transmission electron microscopy (TEM) image in Figure 1b. The NW tip is enlarged with an irregular shape caused by un-optimized consumption of the Ga catalytic droplet after the core-NW growth. Defect-free core-shell NWs with high crystalline quality and regular morphology can be achieved by optimized growth parameters 41 .

NWs were then coated by an uniform layer of amorphous TiO_2 deposited by ALD, confirmed by the energy dispersive X-ray spectroscopy (EDX) composition mapping of Ga and Ti shown in Figure 1c and the composition line scan near the surface shown in Figure 1d, as well as the X-ray photoelectron spectroscopy (XPS) spectra in Supporting Information Figure S1a. The thickness of TiO_2 protection layer is ~7 nm with a high uniformity from the bottom to the tip of the NWs, as shown in Figure 1e~h. The uniform deposition of conformal films with highly

controllable thickness on complex three-dimensional surfaces is a key benefit of ALD growth. The Pt co-catalyst was deposited on the surface of TiO₂ by aerosol assisted chemical vapor deposition (AACVD). Pt formed small particles (<3 nm) which are confirmed by EDX line scans in Figure 1d. The Pt nanoparticles are decorating the surface of the NWs as shown in Figure 1h~k, but the density and size gradually reduce from the tip to bottom, possibly due to the shadowing effect caused by the neighbouring NWs.

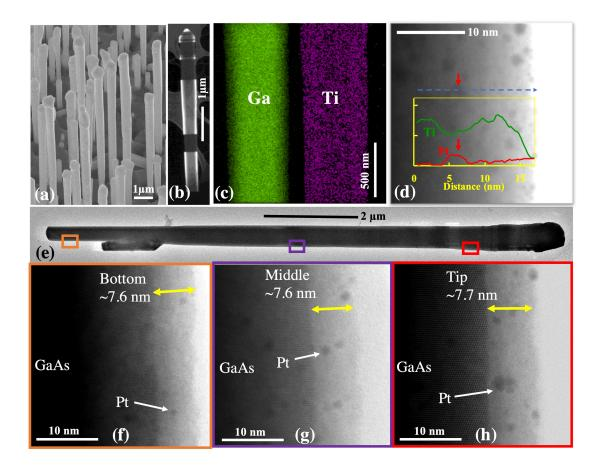


Figure 1. Structure information of GaAs NWs covered by TiO₂ and Pt. (a) Low-magnification SEM images showing the NWs. (b) Low-magnification TEM image of a NW. (c) EDX mapping of Ga and Ti in a NW segment. (d) EDX composition line scan near the NW surface shown in its inset. (e) Low-magnification TEM image showing an entire NW. Higher

magnification TEM images showing the NW/TiO₂ interfaces at the (**f**) bottom, (**g**) middle, and (**h**) tip of the NW marked in (e).

Compact TiO₂ and its influence on optical properties

The influence of TiO₂ on the optical properties of GaAs NWs was analysed by photoluminescence (PL) spectroscopy. Figure 2 shows the PL spectrum of GaAs NWs with and without the TiO₂ layer. With the addition of TiO₂ on the same day after the NW growth, PL emissions from GaAs NWs are quenched by a factor of 2.8, which is typical for type-II heterojunctions that can efficiently separate charge carriers and thereby reduce radiative recombination ¹⁰. As illustrated in the inset of Figure 2, the conduction band (CB) of GaAs is slightly higher than that of TiO₂, therefore electron migration from the NWs to the surface is promoted allowing for efficient water splitting. The valence band of TiO₂ is much lower than that of GaAs, thus forming a favourable barrier to keep holes away from the surface.

When exposed to air, the NW surface can be oxidised to form a native oxide layer (1-2 nm), which act as high-density non-radiative recombination centres, resulting in charge trapping. This can consume a large portion of the photon generated carriers and lead to low light emission. After storing in atmosphere for 14 months, the NWs without TiO_2 protection experienced severe decay and the emission intensity reduced to 13.2%. In contrast, the NWs with a \sim 7 nm TiO_2 protection layer can maintain 91.4% of the emission intensity after storing in the same environment and period. This suggests that the TiO_2 layer has good compactness that can prevent the permeation of oxygen and water, and thus can provide a long-term protection to the NWs' surface.

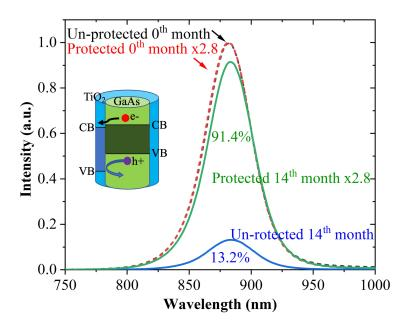


Figure 2. PL spectra from GaAs NWs with and without a TiO₂ protection layer. The TiO₂ protection layer was deposited on the same day of the NW growth. The spectra were taken on the 1st day of NW growth and after 14 months' storage in atmosphere.

Photoelectrochemical Performance

The PEC performance of GaAs NWs photoelectrodes with and without TiO_2 was determined by using them as a photocathode to water splitting and H_2 generation. A three-electrode system, working electrode, Ag/AgCl as reference electrode and Pt as counter electrode, was used. 0.5 M H_2SO_4 (pH = 1) solution was used as electrolyte, with the PEC reaction carried out under 1 sun illumination from AM 1.5 G solar simulator.

As shown in Figure 3a, the un-protected GaAs NW photocathodes have a photocurrent onset potential of ~0.233 V reversible hydrogen electrode (RHE), and a photocurrent density of 0.598 mA/cm² at 0 V vs RHE. As shown in Figure 3b, the protected GaAs NW photocathodes have a slightly larger photocurrent onset potential of ~0.243 V RHE, and a much larger photocurrent

density of 0.87 mA/cm² at 0 V vs RHE – a 45% increase. The increased photocurrent density is due to TiO₂ surface passivation, and the type-II band alignment between TiO₂ and GaAs NWs that are beneficial for efficient carrier separation as discussed above.

A gas chromatograph (GC) system was used to measure the actual H_2 generation rate of the protected NW photocathode when under continuous irradiation with a bias voltage of -0.6 V. As shown in Figure 3c, the generated H_2 volume increased linearly. The theoretical generation value of hydrogen is obtained from the I×t curve by the equation 42 :

$$H_2 = \frac{Q}{2F} = \frac{I \times t}{2F} = \frac{1}{2} \frac{\left(\int_0^t I dt\right)}{F} \tag{1}$$

Where, F is the Faraday constant (96484.34 C/mol), Q is the amount of charge passed in time t, I is the photocurrent. when the current is not constant, the amount of charge passed through the circuit can be estimated by integrating the current over time. The Faraday efficiency can be calculated by the equation:

Faraday efficiency =
$$\frac{\text{Experimential generation value of } H_2}{\text{Theoretical estimated value of } H_2}$$
 (2)

As can be deduced from Figure 3c, the H_2 generation rate was about 22 μ mol/h and is highly stable for the one-hour period measured, which can be further supported by the stable photocurrent in the inset. The photocathode also exhibited a high and stable Faraday efficiency of 91%, which shows that the surface condition is highly favourable for carriers to participate in the water-splitting reaction.

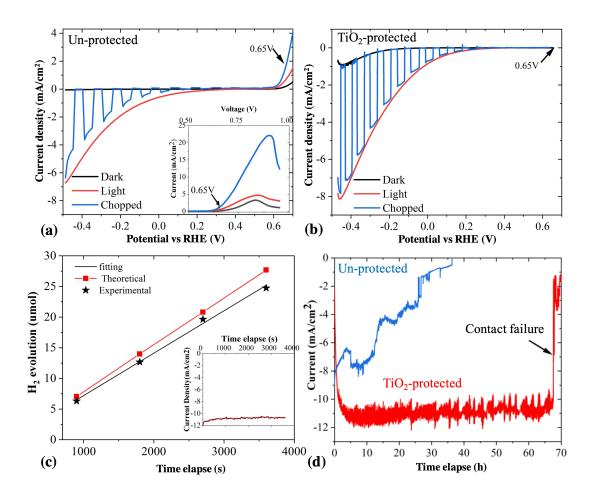


Figure 3. Photoelectrochemical properties of GaAs photocathodes. (a) The J-V curves of unprotected photocathodes and the inset Figure. shows the enlarged of J-V curve above 0.5V vs RHE. (b) TiO₂-protected photocathodes under one sun illumination (AM 1.5 G 100 mW/cm²) in 0.5 M H₂SO₄ electrolyte (pH=1). (c) Experimental and theoretical H₂ evolution of TiO₂-protected photocathodes under continuous illumination (AM 1.5G 100 mW/cm²) (d) Stability of the protected and un-protected photocathodes measured with a bias of -0.6 V and under an AM 1.5 sun illumination.

Photoelectrochemical Stability

The corrosion current of the un-protected NW photocathode is ~2 mA/cm² at 0.65 V vs RHE and increased rapidly with a forward bias as can be seen in Figure 3a and its inset; while the TiO2-protected photocathodes do not show photo-corrosion current at 0.65 V vs RHE, which suggests better stability in the PEC reaction. To further confirm this, a stability test of the hydrogen evolution reaction of the photocathodes was carried out. The hydrogen is uniformly generated on the surface of the test samples, and the hydrogen generation rate is fast and stable when the NWs were in a good state (Supporting Information S2). As shown in Figure 3d, the current density of the un-protected NW photocathode started at about 8.5 mA/cm² under -0.6V vs RHE, then dropped rapidly to ~0 mA/cm² after ~36 hours; while the initial current density of the protected photocathode was ~11 mA/cm² and highly stable over a long duration of 67 hours that is already much longer than other narrow bandgap III-V NW photoelectrodes so far as we know. Beyond this time, no data is available due to the failure of the back contact (Supporting Information S3).

After the stability test, the NWs from the un-protected photocathode were found to have detached from the substrate and bundled together, forming large NW groups and producing areas free of NWs, as can be seen in Figure 4a and b. As can be seen in more detailed in Figure 4c corresponds to the bottom of the NWs, which is highly rough and significantly thinned down to ~50 nm due to the corrosion. NWs with a high-aspect ratio tend to bend and bundle together after removal from liquid due to the capillary force ⁴³. When the NW bottom is very thin, they can break off the substrate when bending. In addition, the other parts of NWs are also corroded during the PEC reaction, and the Pt particles seen to have been washed away in the process as can be seen in Figure 4d. For the protected photocathode, NWs are also bent and bundled,

forming smaller groups of NWs as can be seen in Figure 4e. However, none of the NWs are observed to be broken off from the substrate due to solution etching. The TiO_2 protection layer is still on the surface of NWs with a thickness of \sim 7 nm (Figure 4f), which can be further confirmed by the uniform distribution of Ti from the EDS mapping shown in Figure 4g that were taken at the bottom of NWs. There is no noticeable changes in chemical format of TiO_2 films during PEC water splitting (Supporting Information S1). Besides, the Pt particles are also still present on the surface as can be seen in Figure 4f. Thus, no apparent corrosion from protected NWs was observed.

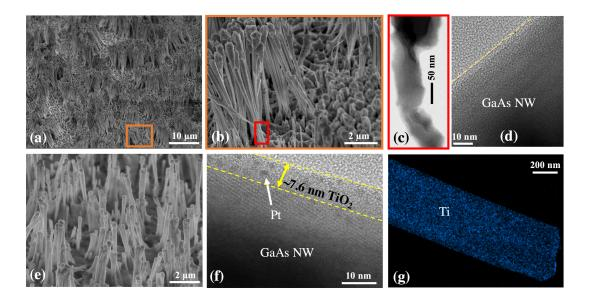


Figure 4. Morphology and structure of GaAs NW photocathodes after stability test. (a)~(d) are from un-protected photocathode. (a) SEM image gives an overall view of the sample surface. (b) higher magnification SEM image of the orange square shown in (a). (c) TEM image showing the bottom of a NW with severe corrosion. (d) TEM image showing the Pt-free surface of the NWs. (e)~(h) are from protected photocathodes. (e) SEM image of the sample surface.

(f) TEM image of NW surface showing GaAs/TiO₂ interface and the Pt particles. (g) is Ti element mapping of the NW bottom.

Conclusion

In this study, the stability of un-protected and protected narrow-bandgap III-V NWs in the PEC reaction was investigated in detail using GaAs NWs. The un-protected NWs suffered from severe corrosion, leading to full failure in the PEC reaction within 35 hours. TiO₂ layer of ~7 nm was used to protect the NWs and to minimize the detrimental corrosion effects. The ALD growth can conformably cover the entire NWs surface with a highly-uniform TiO₂ layer. After storing in atmosphere for 14 months, the protected NWs can still keep 91.4% of its emission intensity, outperforming the un-protected ones that can only maintain 13%. This suggests that the compact TiO₂ film can prevent oxygen and water permeation to the surface of GaAs NWs. The protected GaAs NWs were used as the cathode for PEC water splitting and the photocurrent density improved by 45% to 0.87 mA/cm² at 0V vs RHE due to the surface passivation effect from the TiO₂ layer and the favourable band alignment between GaAs and TiO₂ which improved the charge transfer and reduced the charge recombination at the photocathode. After 67 hours of PEC reaction under continuous simulated solar light illumination, there was no obvious decay of the electrode and the protection layer is still in a very good state. The protected photocathode also shows good faradaic efficiency of ~91%, which suggests that the surface condition is highly favourable for carriers to participate in the water-splitting reaction. These results show that a thin layer of compact TiO₂ can provide superior protection to GaAs NWs,

and addresses for the first time the short stability issue of narrow bandgap III-V NWs and allows them to be practically used in the PEC reaction for significantly longer.

Methods

NW growth: The self-catalysed GaAs NWs were grown directly on p-type Si(111) substrates by solid-source III–V molecular beam epitaxy 44 . The Ga beam equivalent pressure, V/III flux ratio, and substrate temperature were 8.41×10^{-8} Torr, ~ 50 , and ~ 630 °C, respectively. To grow the shell, the Ga droplets were consumed by closing the Ga flux and keeping the group-V fluxes open after the growth of the core. The shells were grown with a Ga beam equivalent pressure, V/III flux ratio, substrate temperature, and growth duration of 8.41×10^{-8} Torr, 86, ~ 500 °C, and 90 mins, respectively. The substrate temperature was measured by a pyrometer. The doping concentration of GaAs p-core, p-shell, and n-shell were 1.6×10^{18} (Be), 1.6×10^{18} (Be), and $1 \times 10^{18} \sim 1 \times 10^{19}$ (Si) cm⁻³, respectively. The thickness ratio of the GaAs p-core, p-shell, and n-shell is 2:3:3. On the p-i-n junction, a layer of ~ 30 nm Al_{0.5}Ga_{0.5}As surface passivation layer and a ~ 10 nm GaAs protection layer were grown with a Si doping concentration of 1×10^{19} cm⁻³.

Scanning Electron Microscope (SEM): The NW morphology was characterised with a Zeiss XB 1540 FIB/SEM system.

Transmission Electron Microscopy (TEM): Simple scraping of the NWs onto a holey carbon support was used to prepare TEM specimens. The TEM measurements were performed with a doubly-corrected ARM200F microscope, operating at 200 kV.

 TiO_2 Deposition: The uniform amorphous TiO_2 film was deposited on the GaAs nanowire at 100° C by applying ALD at the pressure of 1×10^{-2} mbar, using titanium isopropoxide (TTIP) and water as metal and oxygen precursors ⁴⁵. The deposition rate was about 0.48Å/cycle.

Pt Deposition: Pt was applied as a co-catalyst deposited on the surface of GaAs nanowires coated with TiO_2 by the AACVD method to accelerate the hydrogen evolution reaction (HER) rate $^{46-48}$. Aerosols of Pt precursor dissolved in methanol were generated by an ultrasonic humidifier and then the aerosols were transported to the reactor by using nitrogen carrier gas operated by a mass flow controller 49,50 . The deposition was carried out at 350°C with a deposition time 30 minutes.

Photoelectrochemical Measurements (PEC): The PEC properties of the GaAs nanowire photoelectrodes were measured by a three-electrode system composed of a Ag/AgCl reference electrode, Pt counter electrode and GaAs NWs as the photoactive working electrode. The constant potential of the working electrode was controlled by a potentiostat. The electrolyte, $0.5M~H_2SO_4~(pH=1)$ was used as the PEC reaction solution, and the PEC reaction was carried out under 1 AM 1.5 G sun illumination. Stability test of the photocathode was carried out under an AM 1.5 sun illumination. The stability reaction was carried out in a 0.5 mol/L sulfuric acid solution (pH = 1), with a constant potential relative to an RHE equal to 0. A gas chromatograph (GC; Shimadzu GC-2014) was used to measure the hydrogen generation rate. According to the Nernst equation, the measured potential (vs. Ag/AgCl) can be converted into a reversible hydrogen electrode (NHE at pH = 1): $E_{RHE} = E_{Ag/AgCl} + E_{0Ag/AgCl} + 0.059 \times pH$. Generally, at room temperature $E_{0Ag/AgCl} = 0.197~V^{51}$. In order to control photo corrosion, both the PEC test and

the stability test voltage were selected as the safe voltage range -0.733–0.4 V. The photocurrent density (J) and electric potential (V) for a GaAs nanowire Si/GaAs-TiO₂-Pt photocathode was measured by linear scanning voltammetry. The measurement was carried out in the dark, in a chopper, and in continuous light under one sun illumination (AM 1.5 G 100 mW/cm²) ⁵².

Acknowledgements:

The authors acknowledge the support of Leverhulme Trust, EPSRC (grant nos. EP/P000916/1, EP/P000886/1, EP/P006973/1), and EPSRC National Epitaxy Facility. The authors also acknowledge Research Interest limited company for capturing Figure 4f and g.

Competing interests

The authors declare no competing interests.

Additional information

Supplementary information is available for this paper at https://doi.org/

References

- (1) Headley, S. A New Day Dawning. *Youth Stud. Aust.* **2013**, *32* (2), 1–2. https://doi.org/10.1038/443019a.
- (2) Bensaid, S.; Centi, G.; Garrone, E.; Perathoner, S.; Saracco, G. Towards Artificial Leaves for Solar Hydrogen and Fuels from Carbon Dioxide. *ChemSusChem* **2012**, *5* (3), 500–521. https://doi.org/10.1002/cssc.201100661.

- (3) FUJISHIMA, A.; HONDA, K. Electrochemical Photolysis of Water at a Semiconductor Electrode. *Nature* **1972**, *238* (5358), 37–38. https://doi.org/10.1038/238037a0.
- (4) Walter, M. G.; Warren, E. L.; McKone, J. R.; Boettcher, S. W.; Mi, Q.; Santori, E. A.; Lewis, N. S. Solar Water Splitting Cells. *Chem. Rev.* 2010, 110 (11), 6446–6473. https://doi.org/10.1021/cr1002326.
- (5) Jeon, K. J.; Moon, H. R.; Ruminski, A. M.; Jiang, B.; Kisielowski, C.; Bardhan, R.; Urban, J. J. Air-Stable Magnesium Nanocomposites Provide Rapid and High-Capacity Hydrogen Storage without Using Heavy-Metal Catalysts. *Nat. Mater.* 2011, 10 (4), 286–290. https://doi.org/10.1038/nmat2978.
- (6) Chen, J.; Yang, D.; Song, D.; Jiang, J.; Ma, A.; Hu, M. Z.; Ni, C. Recent Progress in Enhancing Solar-to-Hydrogen Efficiency. *J. Power Sources* 2015, 280, 649–666. https://doi.org/10.1016/j.jpowsour.2015.01.073.
- (7) Landman, A.; Dotan, H.; Shter, G. E.; Wullenkord, M.; Houaijia, A.; Maljusch, A.; Grader, G. S.; Rothschild, A. Photoelectrochemical Water Splitting in Separate Oxygen and Hydrogen Cells. *Nat. Mater.* 2017, *16* (6), 646–651. https://doi.org/10.1038/nmat4876.
- (8) Bae, D.; Seger, B.; Vesborg, P. C. K.; Hansen, O.; Chorkendorff, I. Strategies for Stable Water Splitting: Via Protected Photoelectrodes. *Chem. Soc. Rev.* 2017, 46 (7), 1933–1954. https://doi.org/10.1039/c6cs00918b.

- (9) Khaselev, O.; Turner, J. A. A Monolithic Photovoltaic-Photoelectrochemical Device for Hydrogen Production via Water Splitting. *Science* (80-.). **1998**, 280 (5362), 425–427. https://doi.org/10.1126/science.280.5362.425.
- Butson, J. D.; Narangari, P. R.; Lysevych, M.; Wong-Leung, J.; Wan, Y.; Karuturi, S.
 K.; Tan, H. H.; Jagadish, C. InGaAsP as a Promising Narrow Band Gap
 Semiconductor for Photoelectrochemical Water Splitting. ACS Appl. Mater. Interfaces
 2019, 11 (28), 25236–25242. https://doi.org/10.1021/acsami.9b06656.
- (11) Ros, C.; Andreu, T.; Morante, J. R. Photoelectrochemical Water Splitting: A Road from Stable Metal Oxides to Protected Thin Film Solar Cells. *J. Mater. Chem. A* **2020**, 8 (21), 10625–10669. https://doi.org/10.1039/d0ta02755c.
- Zheng, J.; Zhou, H.; Zou, Y.; Wang, R.; Lyu, Y.; Jiang, S. P.; Wang, S. Efficiency and Stability of Narrow-Gap Semiconductor-Based Photoelectrodes. *Energy Environ. Sci.* 2019, 12 (8), 2345–2374. https://doi.org/10.1039/c9ee00524b.
- (13) Abdi, F. F.; Han, L.; Smets, A. H. M.; Zeman, M.; Dam, B.; Van De Krol, R. Efficient Solar Water Splitting by Enhanced Charge Separation in a Bismuth Vanadate-Silicon Tandem Photoelectrode. *Nat. Commun.* **2013**, *4*, 1–7. https://doi.org/10.1038/ncomms3195.
- (14) Fountaine, K. T.; Lewerenz, H. J.; Atwater, H. A. Efficiency Limits for Photoelectrochemical Water-Splitting. *Nat. Commun.* 2016, 7, 1–9. https://doi.org/10.1038/ncomms13706.

- (15) Britto, R. J.; Young, J. L.; Yang, Y.; Steiner, M. A.; Lafehr, D. T.; Friedman, D. J.;
 Beard, M.; Deutsch, T. G.; Jaramillo, T. F. Interfacial Engineering of Gallium Indium
 Phosphide Photoelectrodes for Hydrogen Evolution with Precious Metal and NonPrecious Metal Based Catalysts. *J. Mater. Chem. A* 2019, 7 (28), 16821–16832.
 https://doi.org/10.1039/c9ta05247j.
- Jiang, C.; Moniz, S. J. A.; Wang, A.; Zhang, T.; Tang, J. Photoelectrochemical
 Devices for Solar Water Splitting-Materials and Challenges. *Chem. Soc. Rev.* 2017, 46
 (15), 4645–4660. https://doi.org/10.1039/c6cs00306k.
- Ben-Naim, M.; Britto, R. J.; Aldridge, C. W.; Mow, R.; Steiner, M. A.; Nielander, A.
 C.; King, L. A.; Friedman, D. J.; Deutsch, T. G.; Young, J. L.; Jaramillo, T. F.
 Addressing the Stability Gap in Photoelectrochemistry: Molybdenum Disulfide
 Protective Catalysts for Tandem III–V Unassisted Solar Water Splitting. *ACS Energy Lett.* 2020, *5* (8), 2631–2640. https://doi.org/10.1021/acsenergylett.0c01132.
- Tournet, J.; Lee, Y.; Karuturi, S. K.; Tan, H. H.; Jagadish, C. III–V Semiconductor Materials for Solar Hydrogen Production: Status and Prospects. *ACS Energy Lett*.
 2020, 5 (2), 611–622. https://doi.org/10.1021/acsenergylett.9b02582.
- (19) Lieber, C. M.; Wang, Z. L. F Unctional Nanowires. **2018**, *32* (February 2007), 99–108.
- (20) Yang, P.; Yan, R.; Fardy, M. Semiconductor Nanowire: Whats Next? *Nano Lett.* **2010**, *10* (5), 1529–1536. https://doi.org/10.1021/nl100665r.

- (21) Lohn, A. J.; Li, X.; Kobayashi, N. P. Epitaxial Growth of Ensembles of Indium Phosphide Nanowires on Various Non-Single Crystal Substrates Using an Amorphous Template Layer. *J. Cryst. Growth* 2011, 315 (1), 157–159. https://doi.org/10.1016/j.jcrysgro.2010.08.050.
- Van Dam, D.; Abujetas, D. R.; Paniagua-Domínguez, R.; Sánchez-Gil, J. A.; Bakkers,
 E. P. A. M.; Haverkort, J. E. M.; Gómez Rivas, J. Directional and Polarized Emission
 from Nanowire Arrays. *Nano Lett.* 2015, *15* (7), 4557–4563.
 https://doi.org/10.1021/acs.nanolett.5b01135.
- (23) Krogstrup, P.; Jørgensen, H. I.; Heiss, M.; Demichel, O.; Holm, J. V.; Aagesen, M.; Nygard, J.; Fontcuberta I Morral, A. Single-Nanowire Solar Cells beyond the Shockley-Queisser Limit. *Nat. Photonics* 2013, 7 (4), 306–310. https://doi.org/10.1038/nphoton.2013.32.
- Muskens, O. L.; Rivas, J. G.; Algra, R. E.; Bakkers, E. P. A. M.; Lagendijk, A. Design of Light Scattering in Nanowire Materials for Photovoltaic Applications. *Nano Lett*.
 2008, 8 (9), 2638–2642. https://doi.org/10.1021/nl0808076.
- (25) Garnett, E.; Yang, P. Light Trapping in Silicon Nanowire Solar Cells. *Nano Lett.* 2010, 10 (3), 1082–1087. https://doi.org/10.1021/nl100161z.
- (26) Wen, L.; Zhao, Z.; Li, X.; Shen, Y.; Guo, H.; Wang, Y. Theoretical Analysis and Modeling of Light Trapping in High Efficiency GaAs Nanowire Array Solar Cells. Appl. Phys. Lett. 2011, 99 (14). https://doi.org/10.1063/1.3647847.

- (27) Zhou, B.; Kong, X.; Vanka, S.; Chu, S.; Ghamari, P.; Wang, Y.; Pant, N.; Shih, I.;
 Guo, H.; Mi, Z. Gallium Nitride Nanowire as a Linker of Molybdenum Sulfides and
 Silicon for Photoelectrocatalytic Water Splitting. *Nat. Commun.* 2018, 9 (1).
 https://doi.org/10.1038/s41467-018-06140-1.
- Standing, A.; Assali, S.; Gao, L.; Verheijen, M. A.; Van Dam, D.; Cui, Y.; Notten, P. H. L.; Haverkort, J. E. M.; Bakkers, E. P. A. M. Efficient Water Reduction with Gallium Phosphide Nanowires. *Nat. Commun.* 2015, 6 (May), 1–7.
 https://doi.org/10.1038/ncomms8824.
- (29) Alqahtani, M.; Sathasivam, S.; Alhassan, A.; Cui, F.; Benjaber, S.; Blackman, C.;
 Zhang, B.; Qin, Y.; Parkin, I. P.; Nakamura, S.; Liu, H.; Wu, J. InGaN/GaN Multiple
 Quantum Well Photoanode Modified with Cobalt Oxide for Water Oxidation. ACS
 Appl. Energy Mater. 2018, 1 (11), 6417–6424.
 https://doi.org/10.1021/acsaem.8b01387.
- (30) Alqahtani, M.; Ben-Jabar, S.; Ebaid, M.; Sathasivam, S.; Jurczak, P.; Xia, X.;
 Alromaeh, A.; Blackman, C.; Qin, Y.; Zhang, B.; Ooi, B. S.; Liu, H.; Parkin, I. P.;
 Wu, J. Gallium Phosphide Photoanode Coated with TiO 2 and CoO x for Stable
 Photoelectrochemical Water Oxidation . *Opt. Express* 2019, 27 (8), A364.
 https://doi.org/10.1364/oe.27.00a364.
- (31) Wu, J.; Li, Y.; Kubota, J.; Domen, K.; Aagesen, M.; Ward, T.; Sanchez, A.; Beanland, R.; Zhang, Y.; Tang, M.; Hatch, S.; Seeds, A.; Liu, H. Wafer-Scale Fabrication of Self-Catalyzed 1.7 EV GaAsP Core-Shell Nanowire Photocathode on Silicon Substrates. *Nano Lett.* 2014, 14 (4), 2013–2018. https://doi.org/10.1021/nl500170m.

- (32) Moehl, T.; Suh, J.; Sévery, L.; Wick-Joliat, R.; Tilley, S. D. Investigation of (Leaky)
 ALD TiO2 Protection Layers for Water-Splitting Photoelectrodes. ACS Appl. Mater.
 Interfaces 2017, 9 (50), 43614–43622. https://doi.org/10.1021/acsami.7b12564.
- (33) Chu, S.; Vanka, S.; Wang, Y.; Gim, J.; Wang, Y.; Ra, Y. H.; Hovden, R.; Guo, H.; Shih, I.; Mi, Z. Solar Water Oxidation by an InGaN Nanowire Photoanode with a Bandgap of 1.7 EV. *ACS Energy Lett.* **2018**, *3* (2), 307–314. https://doi.org/10.1021/acsenergylett.7b01138.
- Varadhan, P.; Fu, H. C.; Kao, Y. C.; Horng, R. H.; He, J. H. An Efficient and Stable Photoelectrochemical System with 9% Solar-to-Hydrogen Conversion Efficiency via InGaP/GaAs Double Junction. *Nat. Commun.* **2019**, *10* (1), 1–9. https://doi.org/10.1038/s41467-019-12977-x.
- (35) Cao, S.; Kang, Z.; Yu, Y.; Du, J.; German, L.; Li, J.; Yan, X.; Wang, X.; Zhang, Y.
 Tailored TiO2 Protection Layer Enabled Efficient and Stable Microdome Structured
 P-GaAs Photoelectrochemical Cathodes. Adv. Energy Mater. 2020, 10 (9), 1–7.
 https://doi.org/10.1002/aenm.201902985.
- (36) Hu, S.; Shaner, M. R.; Beardslee, J. A.; Lichterman, M.; Brunschwig, B. S.; Lewis, N. S. Amorphous TiO2 Coatings Stabilize Si, GaAs, and GaP Photoanodes for Efficient Water Oxidation. *Science* (80-.). 2014, 344 (6187), 1005–1009.
 https://doi.org/10.1126/science.1251428.
- (37) Scheuermann, A. G.; Prange, J. D.; Gunji, M.; Chidsey, C. E. D.; McIntyre, P. C. Effects of Catalyst Material and Atomic Layer Deposited TiO2 Oxide Thickness on

- the Water Oxidation Performance of Metal-Insulator-Silicon Anodes. *Energy Environ. Sci.* **2013**, *6* (8), 2487–2496. https://doi.org/10.1039/c3ee41178h.
- (38) Gu, J.; Yan, Y.; Young, J. L.; Steirer, K. X.; Neale, N. R.; Turner, J. A. Water

 Reduction by a P-GaInP2 Photoelectrode Stabilized by an Amorphous TiO2 Coating
 and a Molecular Cobalt Catalyst. *Nat. Mater.* **2016**, *15* (4), 456–460.

 https://doi.org/10.1038/nmat4511.
- (39) Su, J.; Wei, Y.; Vayssieres, L. Stability and Performance of Sulfide-, Nitride-, and Phosphide-Based Electrodes for Photocatalytic Solar Water Splitting. *J. Phys. Chem. Lett.* **2017**, *8* (20), 5228–5238. https://doi.org/10.1021/acs.jpclett.7b00772.
- (40) Zhang, Y.; Aagesen, M.; Holm, J. V.; Jørgensen, H. I.; Wu, J.; Liu, H. Self-Catalyzed GaAsP Nanowires Grown on Silicon Substrates by Solid-Source Molecular Beam Epitaxy. *Nano Lett.* 2013, 13 (8), 3897–3902. https://doi.org/10.1021/nl401981u.
- (41) Zhang, Y.; Fonseka, H. A.; Aagesen, M.; Gott, J. A.; Sanchez, A. M.; Wu, J.; Kim, D.; Jurczak, P.; Huo, S.; Liu, H. Growth of Pure Zinc-Blende GaAs(P) Core-Shell Nanowires with Highly Regular Morphology. *Nano Lett.* 2017, 17 (8), 4946–4950. https://doi.org/10.1021/acs.nanolett.7b02063.
- (42) Alotaibi, B.; Nguyen, H. P. T.; Zhao, S.; Kibria, M. G.; Fan, S.; Mi, Z. Highly Stable Photoelectrochemical Water Splitting and Hydrogen Generation Using a Double-Band InGaN/GaN Core/Shell Nanowire Photoanode. *Nano Lett.* **2013**, *13* (9), 4356–4361. https://doi.org/10.1021/nl402156e.

- (43) Miao, W.; Yao, Y.; Zhang, Z.; Ma, C.; Li, S.; Tang, J.; Liu, H.; Liu, Z.; Wang, D.;
 Camburn, M. A.; Fang, J. C.; Hao, R.; Fang, X.; Zheng, S.; Hu, N.; Wang, X. Micro-/Nano-Voids Guided Two-Stage Film Cracking on Bioinspired Assemblies for High-Performance Electronics. *Nat. Commun.* 2019, 10 (1), 1–8.
 https://doi.org/10.1038/s41467-019-11803-8.
- Zhang, Y.; Sanchez, A. M.; Sun, Y.; Wu, J.; Aagesen, M.; Huo, S.; Kim, D.; Jurczak,
 P.; Xu, X.; Liu, H. Influence of Droplet Size on the Growth of Self-Catalyzed Ternary
 GaAsP Nanowires. *Nano Lett.* 2016, 16 (2), 1237–1243.
 https://doi.org/10.1021/acs.nanolett.5b04554.
- Wilson, R. L.; Simion, C. E.; Blackman, C. S.; Carmalt, C. J.; Stanoiu, A.; Di Maggio,
 F.; Covington, J. A. The Effect of Film Thickness on the Gas Sensing Properties of
 Ultra-Thin TiO2 Films Deposited by Atomic Layer Deposition. *Sensors (Switzerland)*2018, 18 (3). https://doi.org/10.3390/s18030735.
- Li, Y.; Zhang, L.; Torres-Pardo, A.; González-Calbet, J. M.; Ma, Y.; Oleynikov, P.;
 Terasaki, O.; Asahina, S.; Shima, M.; Cha, D.; Zhao, L.; Takanabe, K.; Kubota, J.;
 Domen, K. Cobalt Phosphate-Modified Barium-Doped Tantalum Nitride Nanorod
 Photoanode with 1.5% Solar Energy Conversion Efficiency. *Nat. Commun.* 2013, 4,
 1–2. https://doi.org/10.1038/ncomms3566.
- (47) Chen, S.; Takata, T.; Domen, K. Particulate Photocatalysts for Overall Water Splitting.

 Nat. Rev. Mater. 2017, 2, 1–17. https://doi.org/10.1038/natrevmats.2017.50.

- (48) Promdet, P.; Quesada-Cabrera, R.; Sathasivam, S.; Li, J.; Jiamprasertboon, A.; Guo, J.; Taylor, A.; Carmalt, C. J.; Parkin, I. P. High Defect Nanoscale ZnO Films with Polar Facets for Enhanced Photocatalytic Performance. ACS Appl. Nano Mater. 2019, 2 (5), 2881–2889. https://doi.org/10.1021/acsanm.9b00326.
- (49) Ling, M.; Blackman, C. Growth Mechanism of Planar or Nanorod Structured
 Tungsten Oxide Thin Films Deposited via Aerosol Assisted Chemical Vapour
 Deposition (AACVD). Phys. Status Solidi Curr. Top. Solid State Phys. 2015, 12 (7),
 869–877. https://doi.org/10.1002/pssc.201510047.
- (50) Xia, X.; Taylor, A.; Zhao, Y.; Guldin, S.; Blackman, C. Use of a New Non-Pyrophoric Liquid Aluminum Precursor for Atomic Layer Deposition. *Materials (Basel)*. 2019, 12
 (9). https://doi.org/10.3390/ma12091429.
- (51) Ferrero, G. A.; Preuss, K.; Marinovic, A.; Jorge, A. B.; Mansor, N.; Brett, D. J. L.; Fuertes, A. B.; Sevilla, M.; Titirici, M. M. Fe-N-Doped Carbon Capsules with Outstanding Electrochemical Performance and Stability for the Oxygen Reduction Reaction in Both Acid and Alkaline Conditions. ACS Nano 2016, 10 (6), 5922–5932. https://doi.org/10.1021/acsnano.6b01247.
- (52) Channa, A. I.; Tong, X.; Xu, J. Y.; Liu, Y.; Wang, C.; Sial, M. N.; Yu, P.; Ji, H.; Niu, X.; Wang, Z. M. Tailored Near-Infrared-Emitting Colloidal Heterostructured Quantum Dots with Enhanced Visible Light Absorption for High Performance Photoelectrochemical Cells. *J. Mater. Chem. A* 2019, 7 (17), 10225–10230. https://doi.org/10.1039/c9ta01052a.